



Uncertainty of ENSO-amplitude projections in CMIP5 and CMIP6 models

Goratz Beobide-Arsuaga^{1,2,3} · Tobias Bayr¹ · Annika Reintges¹ · Mojib Latif^{1,4}

Received: 30 June 2020 / Accepted: 22 January 2021
© The Author(s) 2021

Abstract

There is a long-standing debate on how the El Niño/Southern Oscillation (ENSO) amplitude may change during the twenty-first century in response to global warming. Here we identify the sources of uncertainty in the ENSO amplitude projections in models participating in the Coupled Model Intercomparison Phase 5 (CMIP5) and Phase 6 (CMIP6), and quantify scenario uncertainty, model uncertainty and uncertainty due to internal variability. The model projections exhibit a large spread, ranging from increasing standard deviation of up to 0.6 °C to diminishing standard deviation of up to −0.4 °C by the end of the twenty-first century. The ensemble-mean ENSO amplitude change is close to zero. Internal variability is the main contributor to the uncertainty during the first three decades; model uncertainty dominates thereafter, while scenario uncertainty is relatively small throughout the twenty-first century. The total uncertainty increases from CMIP5 to CMIP6: while model uncertainty is reduced, scenario uncertainty is considerably increased. The models with “realistic” ENSO dynamics have been analyzed separately and categorized into models with too small, moderate and too large ENSO amplitude in comparison to instrumental observations. The smallest uncertainties are observed in the sub-ensemble exhibiting realistic ENSO dynamics and moderate ENSO amplitude. However, the global warming signal in ENSO-amplitude change is undetectable in all sub-ensembles. The zonal wind-SST feedback is identified as an important factor determining ENSO amplitude change: global warming signal in ENSO amplitude and zonal wind-SST feedback strength are highly correlated across the CMIP5 and CMIP6 models.

1 Introduction

The El Niño/Southern Oscillation (ENSO) is the strongest interannual climate fluctuation. It originates in the tropical Pacific, has a period of about 4 years, is characterized by basin-wide changes in sea surface temperature (SST) and has global impacts (Philander 1989; McPhaden et al. 2006). Coupled ocean–atmosphere interactions are at the heart of the ENSO mechanism (Bjerknes 1969). The predominantly

easterly trade winds at the surface drive a zonal SST gradient across the equator by accumulating heat in the warm pool region in the west and forming the cold tongue region in the east by coastal and equatorial upwelling. An anomalously strong zonal SST gradient enhances the easterly trade winds, which in turn further strengthens the zonal SST gradient, and vice versa. This positive ocean–atmosphere feedback efficiently enhances initial SST anomalies. El Niño events, the warm extremes of ENSO, for example, go along with anomalously weak trade winds. Similarly, La Niña events, the cold extremes of ENSO, are associated with stronger than normal trade winds (McPhaden et al. 2006). The equatorial upper-ocean heat content acts as a delayed negative feedback in ENSO, and perturbations of heat content and SST are roughly in quadrature (Meinen and McPhaden 2000). Hence, the growth rate of ENSO can be theoretically determined by the total of wind dynamic coupling and the thermal damping (Jin et al. 2006).

Despite the complexity of ENSO dynamics, our understanding of ENSO has considerably improved during the recent years. The fundamental ENSO mechanism has been

✉ Tobias Bayr
tbayr@geomar.de

¹ GEOMAR Helmholtz Centre for Ocean Research Kiel, Düsternbrooker Weg 20, 24105 Kiel, Germany

² Institute of Oceanography, Center for Earth System Research and Sustainability, Universität Hamburg, Hamburg, Germany

³ International Max Planck Research School on Earth System Modelling, Max Planck Institute for Meteorology, Hamburg, Germany

⁴ Faculty of Mathematics and Natural Sciences, Christian Albrechts University, Kiel, Germany

condensed into a conceptual model, termed the recharge oscillator paradigm (Jin 1997). However, each ENSO event is unique, and a large diversity is observed with respect to pattern, amplitude and temporal evolution (Capotondi et al. 2015; Timmermann et al. 2018). Anomalous tropical SSTs affect the deep convection over western tropical Pacific, acting as a Rossby wave source and generating global teleconnections (Trenberth et al. 1998). The teleconnections too can strongly vary from event to event. Thus, understanding ENSO and related impacts remains a major challenge in climate research.

In the past, ENSO has undergone substantial variations in amplitude, frequency and spatial pattern, as demonstrated by instrumental and proxy data (Fedorov and Philander 2000; Yeh and Kirtman 2005; Sun and Yu 2009; McPhaden et al. 2011). ENSO characteristics are believed to have experienced a great variability during the Holocene (Cole 2001; Tudhope et al. 2001; Koutavas et al. 2006; Cobb et al. 2013; McGregor et al. 2013), which is supported by climate models (Khon et al. 2018). Low-frequency modulation of ENSO behavior can be due to internal variability (Wittenberg 2009) as well as external forcing such as increasing atmospheric carbon dioxide (CO₂) levels (Latif et al. 2015).

The future behavior of ENSO under anthropogenic forcing remains an open question. Although ENSO amplitude diversity has been reduced by a factor of two from the Coupled Model Intercomparison Project Phase 3 (CMIP3) to its Phase 5 (CMIP5), ENSO projections for the twenty-first century are still highly uncertain (Meehl et al. 2007; Collins et al. 2010; Stevenson 2012; Taylor et al. 2012; Bellenger et al. 2014; Zheng et al. 2016). In particular, the change in ENSO amplitude remains unclear, even with respect to its sign (Knutson et al. 1997; Solomon et al. 2007; Stocker et al. 2013; Cai et al. 2015; Wang et al. 2019). The inter-model disagreement on the ENSO amplitude change persists in CMIP6 models (Eyring et al. 2016; Brown et al. 2020).

Projecting ENSO amplitude under global warming faces several challenges. First, due to large internal ENSO variability on decadal and centennial time scales, it is hard to untangle the anthropogenic forced signal from natural variability (Wittenberg 2009; Collins et al. 2010). For example, there is an ongoing debate whether the reduction in ENSO variability since 2000 is due to natural variability or anthropogenic forcing (Hu et al. 2013, 2017; Lübbecke and McPhaden 2013; Guan and McPhaden 2016; Maher et al. 2018; Seager et al. 2019; Xu et al. 2019). Second, due to the heterogeneity of ENSO amplitude and dynamics in state-of-the-art climate models, ENSO amplitude projection is strongly model-dependent. In historical simulations with estimates of observed external forcing, ENSO amplitude greatly differs among the CMIP5 (Bellenger et al. 2014) and CMIP6 models (Brown et al. 2020; Planton et al. 2020). Differences in the wind-SST feedback

(Vijayeta and Dommenges 2018) and stochastic forcing explain part of the spread (Wengel et al. 2018). Further, model bias is still an issue. State-of-the-art climate models notoriously exhibit strong disagreements compared to observations with regard to ENSO atmospheric feedbacks and ENSO dynamics (Guilyardi et al. 2009; Lloyd et al. 2009, 2011, 2012; Dommenges et al. 2014; Kim et al. 2014b; Bayr et al. 2018, 2019). The equatorial cold SST bias, which is common to and varies among climate models, shifts the models' mean state into a La Niña-like state with a too westward position of the rising branch of the Pacific Walker Circulation. Linked to that, many climate models underestimate the amplifying wind-SST feedback and damping heat flux-SST feedback, with error compensation between the two (Bayr et al. 2018, 2019, 2020). Moreover, in half of the CMIP5 models the shortwave-SST feedback is erroneously positive, leading to a hybrid of wind stress-driven and shortwave-driven ENSO (Dommenges 2010; Dommenges et al. 2014; Bayr et al. 2019), whereas observations indicate a largely wind stress-forced ENSO (Jin et al. 2006; Bayr et al. 2019). This, in addition to model uncertainty, also may explain part of the spread in twenty-first century ENSO projections. Third, the future greenhouse gas (GHG) emissions or concentrations are unknown. Thus different GHG scenarios need to be taken into consideration that can force quite diverse responses due to the non-linearity of ENSO (Hu et al. 2013).

The projections' uncertainties can be separated into three main components (Hawkins and Sutton 2009). First, the uncertainty due to natural internal variability of the climate system on decadal to centennial time scales. Second, the model uncertainty due to different physics and model biases. Finally, the scenario uncertainty due to unknown future GHG emissions. This method has been applied to global and regional temperature projections (Hawkins and Sutton 2009), and to global warming projections of the Atlantic Meridional Overturning Circulation (Reintges et al. 2017).

The objective of this study is to investigate the uncertainties in twenty-first century ENSO amplitude projections using the CMIP5 and CMIP6 simulations. We quantify the above-mentioned sources of uncertainty. For this purpose, the methodology outlined in Hawkins and Sutton (2009) is used. This study is organized as follows: in Sect. 2, we describe the data and methods used in this paper. Section 3 provides an analysis of the ENSO amplitude and decadal variability in the CMIP5 and CMIP6 model ensembles. In Sect. 4, the sources of uncertainty in the ENSO amplitude projections are investigated. The causes of ENSO amplitude change are addressed in Sect. 5. The main results are summarized and discussed in Sect. 6.

2 Data and methods

2.1 Data

The data used in this study is from the World Climate Research Programme's (WCRP's) CMIP5 and CMIP6 ensembles. We analyze the total output of 56 climate models, 36 from CMIP5 and 20 from CMIP6. Pre-industrial control runs are used to study the natural internal variability, which are compared to Hadley Centre Sea Ice and Sea Surface Temperature v1.1 (HadISST) and NOAA Extended Reconstruction Sea Surface Temperature v3b (ERSST) data sets extending between 1870–2017 and 1854–2015, respectively (Rayner et al. 2003; Smith and Reynolds 2003). Further, models' historical runs and projections under two different radiative forcing scenarios, known as Representative Concentration Pathways (RCP4.5 and RCP8.5) for CMIP5 and Shared Socioeconomic Pathways (SSP2-4.5 and SSP5-8.5) for CMIP6, are investigated. CMIP5 models are forced with historical forcing up to 2005, while CMIP6 models are forced by historical forcing up to 2014. For both ensembles, we define a consistent historical period of 1900–2005 and projection period of 2005–2099. The output of 35 models is available for RCP4.5 and 36 models for RCP8.5 (Table 1), and the output of 20 models for SSP2-4.5 and SSP5-8.5 (Table 2).

As most climate models fail to simulate realistic ENSO dynamics (e.g., due to a cold equatorial SST bias and underestimated ENSO atmospheric feedbacks), we follow the study of Bayr et al. (2019) and create a sub-ensemble of models with strong ENSO atmospheric feedbacks (hereafter “Strong”). CMIP5 and CMIP6 model's atmospheric feedbacks are compared to ERA-Interim and ERA40 data sets (Uppala et al. 2005; Dee et al. 2011). Although the ENSO atmospheric feedbacks are underestimated even in the “Strong” sub-ensemble, it is supposed to provide the most reliable results. In most climate models, error compensation is observed between an underestimated amplifying wind-SST feedback and underestimated damping heat flux-SST feedback (Bayr et al. 2018). In particular, the underestimated positive wind-SST feedback is compensated by an erroneously positive shortwave-SST feedback. As a result, ENSO in these models is a hybrid of wind-driven and shortwave-driven dynamics (Bayr et al. 2019). It is questionable if models with biased ENSO dynamics under present-day conditions can provide useful projections of ENSO amplitude under global warming. This is why the “Strong” sub-ensemble is defined (indicated in italics in Table 1 and Table 2).

Table 1 Coupled Model Intercomparison Project-Phase 5 (CMIP5) data availability for two representative concentration pathway (RCP) scenarios. Models of the “Strong” sub-ensemble are shown in italics. Models are further divided into “High”, “Moderate” and “Low” interannual and decadal ENSO amplitude variability

		RCP 4.5	RCP 8.5	ENSO amplitude
1	ACCESS1.0	X	X	Moderate
2	ACCESS1.3	X	X	Moderate
3	BCC-CSM1.1	X	X	Low
4	BCC-CSM1.1(M)	X	X	High
5	BNU-ESM	X	X	High
6	CanESM2	X	X	Moderate
7	<i>CCSM4</i>	X	X	High
8	<i>CESM1(BGC)</i>	X	X	High
9	<i>CESM1(CAM5)</i>	X	X	Moderate
10	<i>CMCC-CM</i>	X	X	Low
11	<i>CMCC-CMS</i>	X	X	Moderate
12	<i>CNRM-CM5</i>	X	X	Moderate
13	CSIRO-Mk3.6.0	X	X	Moderate
14	FGOALS-g2	X	X	Moderate
15	FGOALS-s2		X	High
16	GFDL-CM3	X	X	High
17	GFDL-ESM2G	X	X	Moderate
18	<i>GFDL-ESM2M</i>	X	X	High
19	GISS-E2-H	X	X	High
20	GISS-E2-H-CC	X	X	Moderate
21	<i>GISS-E2-R</i>	X	X	Low
22	<i>GISS-E2-R-CC</i>	X	X	Low
23	HadGEM2-CC	X	X	Low
24	HadGEM2-ES	X	X	Moderate
25	INM-CM4	X	X	Low
26	IPSL-CM5A-LR	X	X	Moderate
27	IPSL-CM5A-MR	X	X	Low
28	<i>IPSL-CM5B-LR</i>	X	X	Moderate
29	<i>MIROC5</i>	X	X	High
30	MIROC-ESM	X	X	Low
31	MIROC-ESM-CHEM	X	X	Low
32	MPI-ESM-LR	X	X	Moderate
33	MPI-ESM-MR	X	X	Low
34	MRI-CGCM3	X	X	Low
35	<i>NorESM1-M</i>	X	X	Moderate
36	<i>NorESM1-ME</i>	X	X	High

Italics indicate models of the “Strong” sub-ensemble. Models are further divided into “High”, “Moderate” and “Low” interannual and decadal ENSO amplitude variability

2.2 Realistic ENSO dynamic models

The CMIP5 (crosses) and CMIP6 (triangles) models exhibit a large spread in the historical zonal wind stress-SST and net heat flux-SST feedbacks (Fig. 1a), which are calculated by regression of zonal wind stress anomalies in the

Table 2 Coupled Model Intercomparison Project-Phase 6 (CMIP6) data availability for two shared socioeconomic pathway (SSP) scenarios. Models of the “Strong” sub-ensemble are shown in italics. Models are further divided into “High”, “Moderate” and “Low” interannual and decadal ENSO amplitude variability

	SSP2-4.5	SSP5-8.5	ENSO amplitude	
37	ACCESS-CM2	X	X	Moderate
38	ACCESS-ESM-1.5	X	X	Low
39	AWI-CM-1.1-MR	X	X	High
40	BCC-CSM2-MR	X	X	High
41	<i>CAMS-CSM1.0</i>	X	X	High
42	<i>CESM2-WACCM</i>	X	X	High
43	<i>FGOALS-F3-L</i>	X	X	High
44	FGOALS-G3	X	X	High
45	GFDL-CM4	X	X	Moderate
46	GFDL-ESM4	X	X	High
47	INM-CM4.8	X	X	Low
48	INM-CM5.0	X	X	Low
49	IPSL-CM6A-LR	X	X	High
50	<i>MIROC6</i>	X	X	High
51	MPI-ESM1.2-h	X	X	Moderate
52	MPI-ESM1.2-LR	X	X	High
53	<i>MRI-ESM2.0</i>	X	X	Moderate
54	NESM3	X	X	Moderate
55	NorESM2-LM	X	X	High
56	<i>NorESM2-MM</i>	X	X	High

Italics indicate models of the “Strong” sub-ensemble. Models are further divided into “High”, “Moderate” and “Low” interannual and decadal ENSO amplitude variability

Niño4 region (160° E–150° W, 5° N–5° S) and net heat flux anomalies in the combined Niño3 (150° W–90° W, 5° N–5° S) and Niño4 region on SST anomalies (SSTA) in the Niño3.4 region (170° W–120° W, 5° N–5° S). The wind stress and SST anomalies are computed relative to a 30-year running window. Models with strongest wind stress-SST feedback show a stronger net heat flux-SST feedback with a correlation of -0.55 . As mentioned above, we group the models according to their ENSO feedback strength, and a sub-ensemble of models with strong ENSO atmospheric feedbacks (“Strong”) is created (red crosses and triangles in Fig. 1a). In general, these also are the models with a reduced equatorial cold SST bias (Fig. 1b) and with the most non-linear ENSO behavior (Fig. 1c), in agreement with recent studies (Cai et al. 2020; Hayashi et al. 2020). All other models reside in the “Weak” sub-ensemble. This allows us to analyze separately the models with realistic and biased ENSO dynamics.

2.3 ENSO amplitude

ENSO amplitude is calculated as the running standard deviation (STD) of SSTA over the Niño3.4 region. Because our focus is the long-term ENSO amplitude evolution, we remove its short-term variability. For this purpose, 10, 20 and 30-year running STD has been tested with SSTA from ERSST and HadISST. SSTA have been calculated relative to the climatological mean of each running window. The evolution of the ENSO amplitude in HadISST when calculating either the 10 or 20-year running STD exhibits still considerable variability on intradecadal timescales (Fig. 2a, b). In contrast, the intradecadal fluctuations are much reduced when applying a 30-year running filter (Fig. 2c). Identical behavior has been obtained when using ERSST (not shown). Hence, a 30-year running filter has been used in the subsequent analysis to compute the decadal ENSO amplitude variability.

2.4 Sources of uncertainty

The uncertainty analysis follows the approach of Hawkins and Sutton (2009) with the adaptations made by Reintges et al. (2017). According to Hawkins and Sutton (2009), the total uncertainty can be divided into three sources: internal variability, model and scenario uncertainty. Since a 30-year running filter is applied, internal variability is basically retained on timescales of decadal and longer.

In the following uncertainty analysis, the variable x in (1) represents the ENSO amplitude, which depends on the scenario (s), model (m), and time (t).

$$x = x(s, m, t) \quad (1)$$

We consider low-pass filtered values of ENSO amplitude X and decompose it into the internal long-term variability ϵ and the long-term trend X_f :

$$X(s, m, t) = X_f(s, m, t) + \epsilon(s, m, t) \quad (2)$$

A common way to estimate the long-term trend X_f from each model is to compute the mean over an ensemble of simulations performed with different initial conditions but identical external forcing (Maher et al. 2018). However, only one realization from each model is available, so that instead, a polynomial fit calculated over 1900 to 2099 is used to estimate X_f . The internal variability ϵ is obtained by:

$$\epsilon(s, m, t) = X(s, m, t) - X_f(s, m, t) \quad (3)$$

The response to the anthropogenic forcing over the period 2005–2099, x_f , is estimated from each model with the aid of the corresponding X_f . We subtract the historical average i

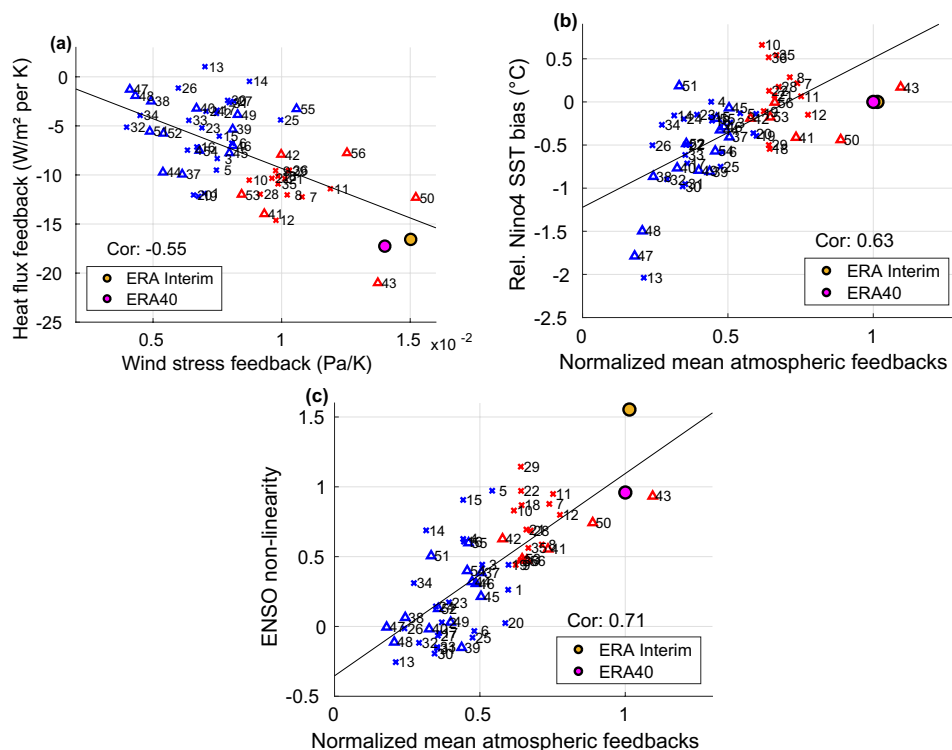


Fig. 1 For individual CMIP5 and CMIP6 models and reanalysis products: **a** net heat flux feedback, defined as regression of net heat flux in Niño3 and Niño4 on SST in Niño3.4 on the y-axis, vs. the zonal wind stress feedback, defined as regression of zonal wind stress in Niño4 region on SST in Niño3.4 region on the x-axis; **b** atmospheric feedback strength (average of wind stress and heat flux feedback, after normalizing each by the average reanalysis value) on x-axis vs. relative SST bias in the Niño4 region (model output SST minus observed SST, after subtracting the tropical Pacific area mean SST from each);

c atmospheric feedback strength (average of wind stress and heat flux feedback, after normalizing each by the average reanalysis value) on x-axis vs. ENSO non-linearity, computed as the difference between Niño3 and Niño4 SSTA skewness; crosses indicate CMIP5 models and triangles CMIP6 models; the red colored symbols indicate models with strong atmospheric feedbacks and realistic ENSO dynamics, called “Strong” sub-ensemble; the blue colored symbols indicate models with weak atmospheric feedbacks, called “Weak” sub-ensemble; the correlation with a 95% confidence level is shown

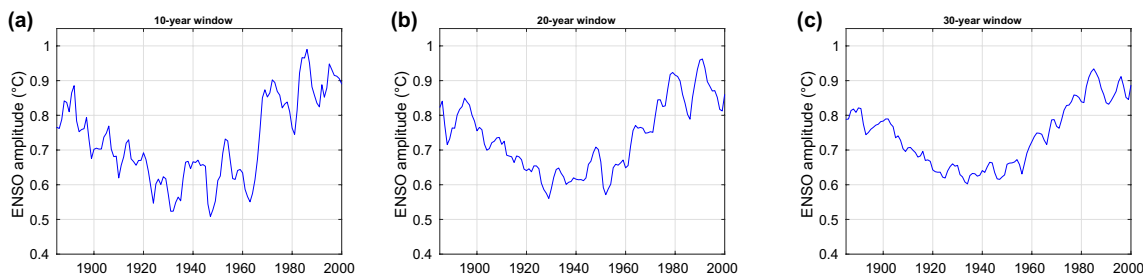


Fig. 2 ENSO amplitude defined as the running standard deviation of Niño3.4 SSTA in HadISST obtained with: **a** 10-year, **b** 20-year and **c** 30-year window

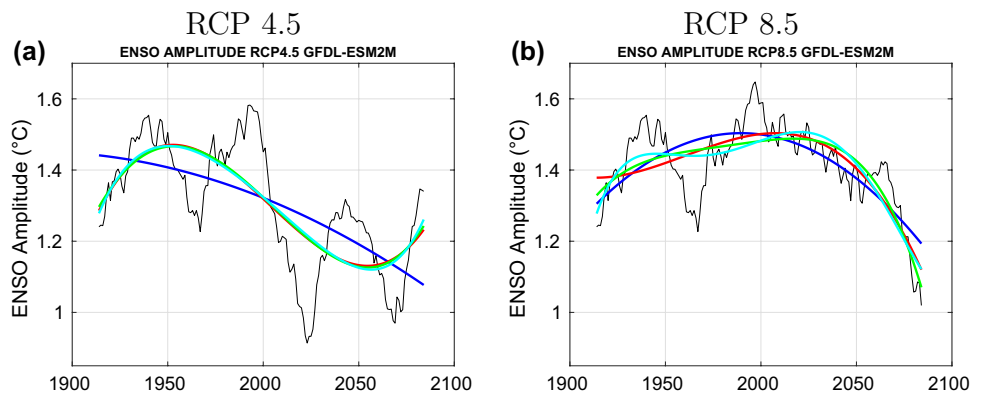
taken over the period 1979–2005 to the projected long-term trend X_{fp} :

$$x_f(s, m, t) = X_{fp}(s, m, t) - i(s, m) \tag{4}$$

Which polynomial fit should be used to represent the long-term trend, and hence, the response to the

anthropogenic forcing? On the one hand, choosing a too high order of the polynomial fit would artificially decrease the level of internal variability. On the other hand, the order of the fit must be high enough to adequately describe the nonlinear externally forced trend. Figure 3 depicts the polynomial fits of the 2nd, 3rd, 4th and 5th order calculated from the GFDL-ESM2M model. Under strong

Fig. 3 Historical and projected ENSO amplitude for the GFDL-ESM2M model (black) with 2nd (blue), 3rd (red), 4th (green) and 5th (cyan) order polynomial fits: in **a** for RCP4.5 and in **b** RCP8.5 scenario



external forcing (RCP8.5), the different orders yield a similar pattern. However, under weak forcing (RCP4.5), only the 2nd order seems to adequately capture the forced trend. Therefore, the 2nd order fit has been chosen. We note in this context that ENSO amplitude can vary internally on multidecadal and centennial time scales (Li et al. 2013). The key results of the uncertainty analysis, however, remain very similar if a higher-order polynomial fit is used.

Using the long-term signal anomaly $x_f(4)$, we can compute the spread between the model projections and then average it over the three scenarios. This will be our inter-model uncertainty that is time-dependent (5).

$$M(t) = \frac{1}{N_s} \cdot \sum_s std_m(x_f(s, m, t)) \tag{5}$$

Next, by averaging x_f over all models for each scenario and computing the spread within the two of them, we get the scenario uncertainty that also is time-dependent (6).

$$S(t) = std_s\left(\frac{1}{N_m} \cdot \sum_m x_f(s, m, t)\right) \tag{6}$$

Last, by computing the spread of each model’s internal variability over time, and then averaging over all models and scenarios, we obtain the internal variability uncertainty, which is independent of time (7).

$$I = \frac{1}{N_s} \cdot \sum_s \frac{1}{N_m} \cdot \sum_m std_i(\epsilon(s, m, t)) \tag{7}$$

The time evolution of the internal variability has been estimated, with the conclusion that it does not show any relevant differences between different periods (Fig. 4).

To test whether the global warming signal in ENSO amplitude is statistically significant, we use the signal-to-noise ratio SNR (8). The average of x_f over all models and scenarios corresponds to the signal, G (9), and the noise to the 95th percentile of the standard normal distribution $q_{c/2}$

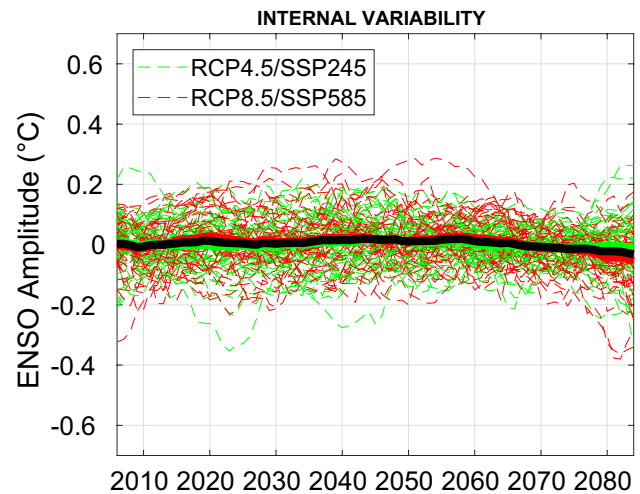


Fig. 4 Internal long-term ENSO amplitude variability for each model and scenario, defined as the difference between the ENSO amplitude and the polynomial fit: green for RCP4.5/SSP2.4.5 scenario and red for RCP8.5/SSP5.8.5 scenario; thin dashed lines correspond to individual model simulations and thick solid lines to the scenario means; black solid line is the mean over all simulations

multiplied by total uncertainty T (10). If the ratio is greater than unity the climate signal is considered detectable.

$$SNR(t) = \frac{G(t)}{q_{c/2} \cdot T(t)} \tag{8}$$

$$G(t) = \frac{1}{N_s} \cdot \sum_s \frac{1}{N_m} \cdot \sum_m x_f(s, m, t) \tag{9}$$

$$T(t) = M(t) + S(t) + I \tag{10}$$

Finally, in order to identify possible origins of the uncertainties, two factors have been considered: the projected mean zonal SST gradient and wind-SST feedback. The mean zonal SST gradient is defined as the temperature difference between the Niño4 and Niño1 + 2 (90° W–80° W, 0°–10°

S) regions relative to the tropical Pacific (120° E–80° W, 15° N–15° S) averaged temperatures. The wind-SST feedback is defined as described above. A 30-year low-pass filter has been applied to the zonal SST gradient and the wind feedback has been computed relative to a 30-year running window. The same methodology as that used for the ENSO amplitude is applied to obtain the global warming signal of the zonal SST gradient and wind-SST feedback. Then, we relate the inter-model spread of the projected ENSO amplitude change to the two factors at the end of the twenty-first century.

3 ENSO amplitude and decadal variability

First, we investigate the ENSO amplitude and its decadal variability in the preindustrial control simulations. The Niño3.4 SSTA is homogenized to the length of 240 years. We have computed the standard deviation of the decadal ENSO amplitude and plotted it against the standard deviation of the interannual Niño3.4 SSTA (Fig. 5). There is a positive relationship with a correlation coefficient of 0.64: models with large (small) interannual Niño3.4 SSTA variability tend to show strong (weak) decadal ENSO amplitude variations. Further, there is a large spread between the models, from much lower to much higher interannual and decadal variability relative to observations. We divide the models into 3 main sub-ensembles: (1) models with high interannual and decadal ENSO variability (“High” sub-ensemble, red squares and triangles), (2) models with low

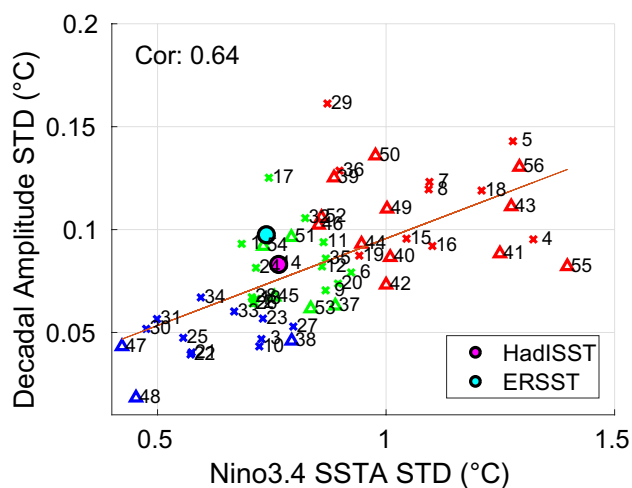


Fig. 5 Pre-industrial interannual Niño3.4 SSTA standard deviation on the x-axis vs. decadal Niño3.4 SSTA standard deviation on the y-axis. Models are grouped into “High” (red), “Moderate” (green) and “Low” (blue) interannual and decadal ENSO variability models; crosses indicate CMIP5 models and triangles CMIP6 models; HadISST and ERSST data sets are shown in magenta and cyan, respectively; the correlation with a 95% confidence level is shown

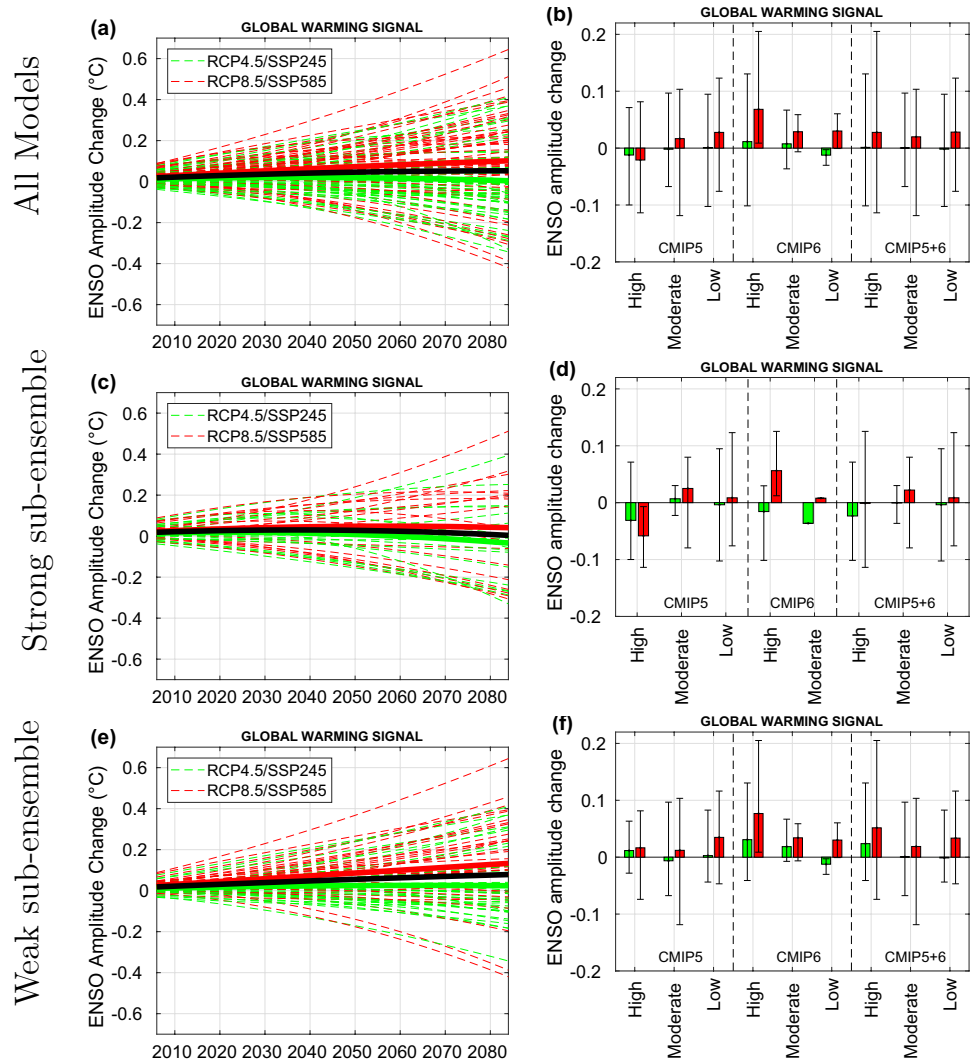
interannual and decadal ENSO variability (“Low” sub-ensemble, blue squares and triangles), and (3) models with the closest variability to observations, moderate interannual and decadal ENSO variability (“Moderate” sub-ensemble, green squares and triangles). Although there is a quite strong linear relationship between interannual and decadal ENSO variability, we consider both the interannual and the decadal ENSO variability for defining the sub-ensembles. If we would only use interannual ENSO variability, we would mix models with different decadal ENSO variability: for instance, we would add several models with unrealistically low decadal ENSO variability as “Moderate”.

4 Global warming signal of the ENSO amplitude and its uncertainties

Figure 6 depicts the global warming signal of the ENSO amplitude. Dashed thin lines in Fig. 6a) represent the individual model simulations for RCP4.5/SSP2-4.5 and RCP8.5/SSP5-8.5 in green and red, respectively. The thick green and red solid lines correspond to the scenario averages and the black solid line to the total scenario and model mean. The strong model disagreement in ENSO amplitude change towards the end of the twenty-first century is clearly visible. The strongest forcing scenario, RCP8.5/SSP5-8.5, contains most of the positive ENSO amplitude changes, while the RCP4.5/SSP2-4.5 simulations are equally balanced between the positive and negative change of the amplitude. The scenario average shows a positive global warming signal for the strongest forcing case and a signal close to zero for RCP4.5/SSP2-4.5 scenario. The total scenario and model mean (thick black line) lays between the two scenario means, showing a slight increase of the ENSO amplitude.

In Fig. 6b), we divide the global warming signal averages for the end of the twenty-first century (RCP4.5/SSP2-4.5 green, RCP8.5/SSP5-8.5 red) into models with high interannual and decadal ENSO variability, moderate interannual and decadal ENSO variability and low interannual and decadal ENSO variability. Vast climate sensitivity differences are present between CMIP models, which has been incremented for the latest phase, CMIP6 (Andrews et al. 2012; Meehl et al. 2020). Prior the sub-ensemble mean, each model’s ENSO amplitude change is divided by the global mean temperature difference between 2050–2099 and 1920–1970 under RCP8.5/SSP5-8.5. Under RCP4.5/SSP2-4.5, CMIP5’s and CMIP6’s forced signal in all three sub-ensembles is close to zero. Under RCP8.5/SSP5-8.5, there are noticeable differences. While CMIP5 models with high decadal ENSO variability project by the end of the twenty-first century a decrease in ENSO amplitude, the “Moderate” and “Low” sub-ensembles show an increase in ENSO amplitude. However, the

Fig. 6 Global warming signal of the ENSO amplitude calculated by subtracting the historical long-term trend (1979–2005) to the projected long-term trend (2005–2099) in **a**, **c**, **e** and to the end of the projected long-term trend (2099) in **b**, **d**, **f**; in **a** individual simulations (dashed lines), RCP4.5/SSP2-4.5 scenario mean (solid green line), RCP8.5/SSP5-8.5 scenario mean (solid red line) and mean over all simulations (solid black line); in **b** mean over “High”, “Moderate” and “Low” sub-ensembles, for RCP4.5/SSP2-4.5 (green) and RCP8.5/SSP5-8.5 (red) scenarios after dividing each model by its climate sensitivity, computed as the global mean temperature difference between 2050–2099 and 1920–1970 under RCP8.5/SSP5-8.5 scenario; error bars show the maximum and minimum value for each sub-ensemble; in **c**, **d** same as **a**, **b**, but here for the “Strong” sub-ensemble; in **e**, **f** same as **a**, **b**, but here for the “Weak” sub-ensemble



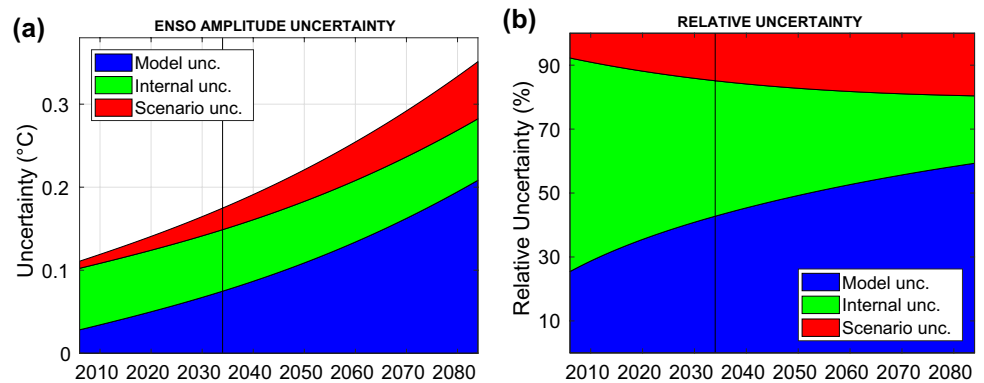
error bars, representing the maximum and minimum values, show a large spread between approximately ± 0.1 . The three sub-ensembles of CMIP6 models on the other hand agree on the increase of ENSO amplitude. The strongest mean ENSO amplitude change is for “High” sub-ensemble. The error bars show a wide range of positive ENSO amplitude changes. It is important to note that we show the result for 20 CMIP6 models, while CMIP5 contains 36 models. At the time of our research, the output of 20 CMIP6 models was available for the variables and scenarios we use. Considering the large spread shown by CMIP5 models, it is possible that 20 models do not represent the full inter-model spread of CMIP6 models. The combination of CMIP5 and CMIP6 leads to an average positive ENSO amplitude change for “High”, “Moderate” and “Low” sub-ensembles.

When only considering the models with strong ENSO atmospheric feedbacks (Fig. 6c, d), the strongest positive and negative ENSO amplitude changes are reduced, shifting

the RCP4.5/SSP2-4.5 scenario and the total means slightly towards negative values (Fig. 6c). The RCP4.5/SSP2-4.5 scenario generally projects a decrease of the mean ENSO amplitude over the sub-ensembles (Fig. 6d). In the RCP8.5 scenario, the CMIP5 “High” sub-ensemble shows a stronger decrease of the ENSO amplitude than in RCP4.5. In contrast, CMIP6 models disagree on the sign of the ENSO amplitude change between the two scenarios. The combination of CMIP5 and CMIP6 sub-ensembles are not able to show any consistent result of global warming signal of ENSO amplitude.

Looking into models with weak ENSO atmospheric feedbacks (Fig. 6e, f), both scenario means and total mean point towards an increase of ENSO amplitude (Fig. 6e). The strongest projected ENSO amplitude change is shown by the RCP8.5/SSP5-8.5 scenario: all sub-ensembles agree on the increase of ENSO amplitude under the strongest forcing scenario for both CMIP5 and CMIP6 ensembles (Fig. 6f). In addition, when comparing to strong ENSO atmospheric

Fig. 7 **a** ENSO amplitude uncertainty divided into model (blue), internal variability (green) and scenario uncertainty (red); in **b** relative uncertainties; solid vertical line represents where model uncertainty becomes larger than internal variability uncertainty



feedback models, the positive ENSO amplitude change is stronger in all sub-ensembles with weak ENSO atmospheric feedbacks except for “Moderate” in CMIP5.

We next quantify and identify the main sources of uncertainty in the projections (Fig. 7). The total uncertainty increases towards the end of the twenty-first century from 0.11 °C to approximately 0.35 °C. In the first three decades, the most important source of uncertainty is the internal decadal variability (green). The internal variability uncertainty amounts to approximately 0.07 °C, corresponding to around 65% of the total uncertainty at the beginning of the projection. After 2034, the main uncertainty source is model uncertainty (blue). It exceeds 0.21 °C by 2100, which corresponds to roughly 60% of the total uncertainty. The scenario uncertainty (red) is of similar magnitude as the internal-variability uncertainty at the end of the twenty-first century. However, it is the smallest uncertainty source at all times. We note that the scenario uncertainty is the largest contribution to the total uncertainty by 2100 when analyzing projections of globally averaged surface temperature, doubling the surface temperature warming from RCP4.5 to RCP8.5, and from SSP2-4.5 to SSP5-8.5 (Knutti and Sedláček 2013; Gidden et al. 2019).

We repeat the uncertainty analysis for CMIP5, CMIP6 and all sub-ensembles, which have been defined above: “Strong”, “Weak”, “High”, “Low” and “Moderate”. We also use the combined selection of “Strong” with “Moderate” sub-ensembles, as the models of this sub-ensemble are closest to observed ENSO in terms of amplitude variability and atmospheric feedback strength. In Fig. 8a we show the results of the uncertainty analysis, and in Fig. 8b) the signal-to-noise ratio, both towards the end of the twenty-first century. Model uncertainty is the largest contributor to the total uncertainty in all sub-ensembles. This result again stresses the importance of the model uncertainty in global warming projections of ENSO amplitude. From CMIP5 to CMIP6 the model uncertainty is reduced, while the scenario uncertainty is largely increased leading to an increase of total uncertainty. The smallest total and model uncertainties

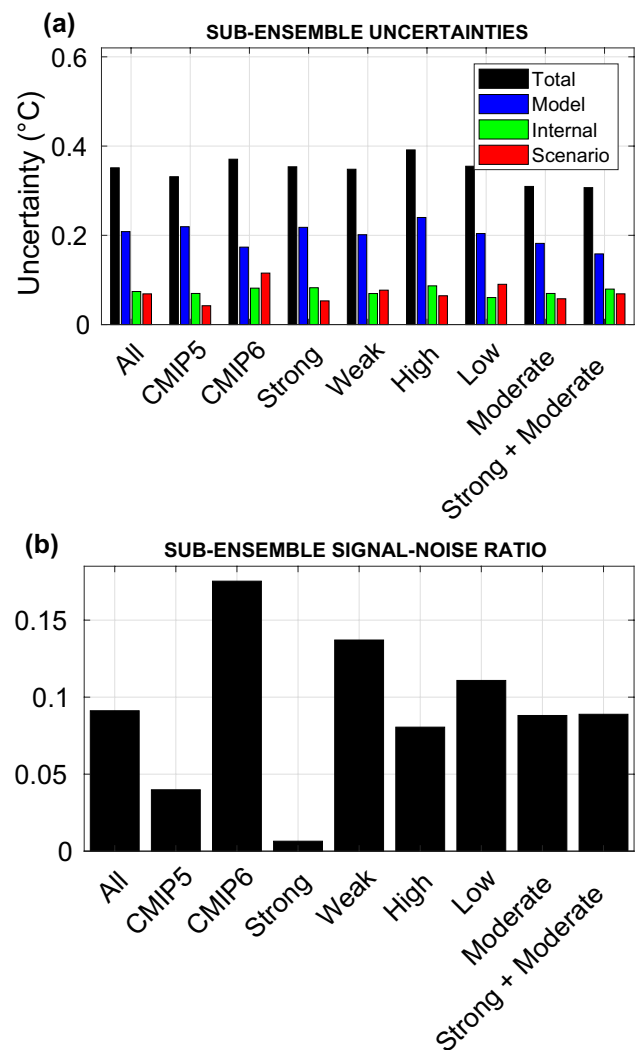


Fig. 8 **a** Total (black), model (blue), internal variability (green) and scenario (red) uncertainties at the end of the projection, year 2099, and **b** signal-to-noise ratio for: all models, CMIP5 models, CMIP6 models, “Strong”, “Weak”, “High”, “Low” and “Moderate” sub-ensembles, and the combination of “Strong” and “Moderate” sub-ensembles

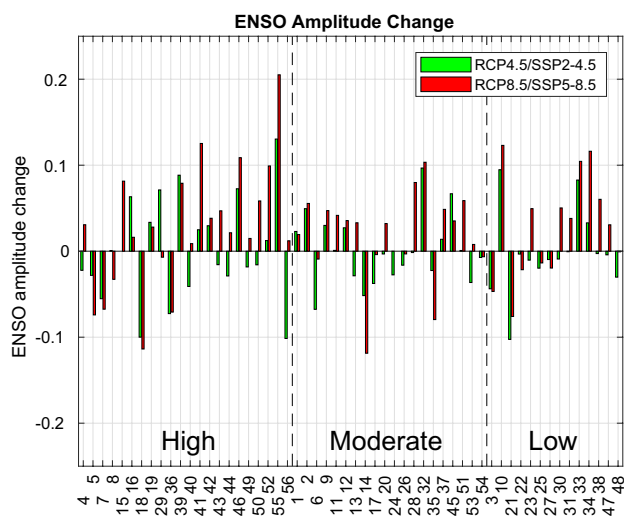


Fig. 9 ENSO amplitude change between 2005 and 2099, computed as a change of the long-term trend, divided by the climate sensitivity of each model, computed as the global mean temperature difference between 2050–2099 and 1920–1970 under RCP8.5/SSP5-8.5 scenario; vertical dashed lines divide from the left to the right; “High”, “Moderate” and “Low” ENSO amplitude sub-ensembles, respectively

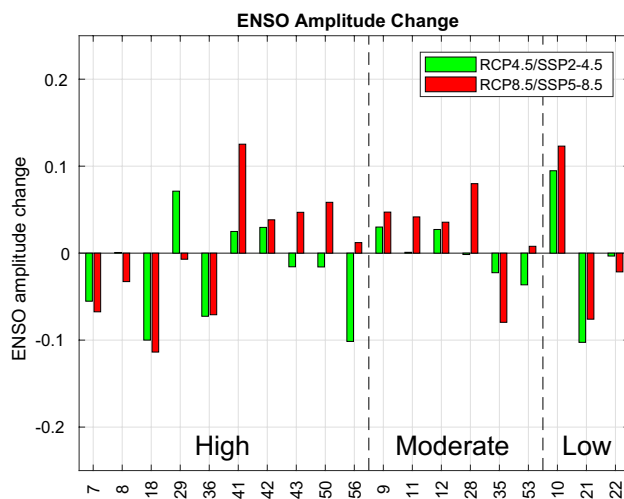


Fig. 10 Same as Fig. 9, but here for the “Strong” sub-ensemble

are observed when combining “Strong” and “Moderate” sub-ensembles. However, even restricting the models to this sub-ensemble does lower the total uncertainty only by $0.045\text{ }^{\circ}\text{C}$ (13%) and model uncertainty by $0.05\text{ }^{\circ}\text{C}$ (24%) in comparison to considering all models ($0.35\text{ }^{\circ}\text{C}$ and $0.21\text{ }^{\circ}\text{C}$, respectively). Further, the signal-to-noise ratio (Fig. 8b) does not exceed the value of unity for any sub-ensemble, which means that a global warming signal in ENSO amplitude cannot be detected with high statistical significance.

We depict the change in ENSO amplitude by the end of the twenty-first century for “High”, “Moderate” and “Low” for all

models in Fig. 9 and for “Strong” in Fig. 10. In Fig. 9 the models within each sub-ensemble largely disagree. Although the projected ENSO amplitude changes in “Strong” are reduced, there is no consistency within the sub-ensembles (Fig. 10). Under the strongest scenario, models in “High” (left group in Fig. 10) agree on a reduced ENSO amplitude for CMIP5 (models 7–36), while for CMIP6 models show an increase of ENSO amplitude (41–56). On the other hand, five out six models in “Moderate” (central group in Fig. 10) point towards an increase under RCP8.5/SSP5-8.5, except for the NorESM1-M model (number 35). In “Low”, there only are three models and it is hard to derive a conclusion. In summary, although models with the most realistic ENSO dynamics and with closest ENSO amplitudes to observations generally point towards an increase of ENSO amplitude, the global warming signal is still robustly undetectable due to the large inter-model disagreements.

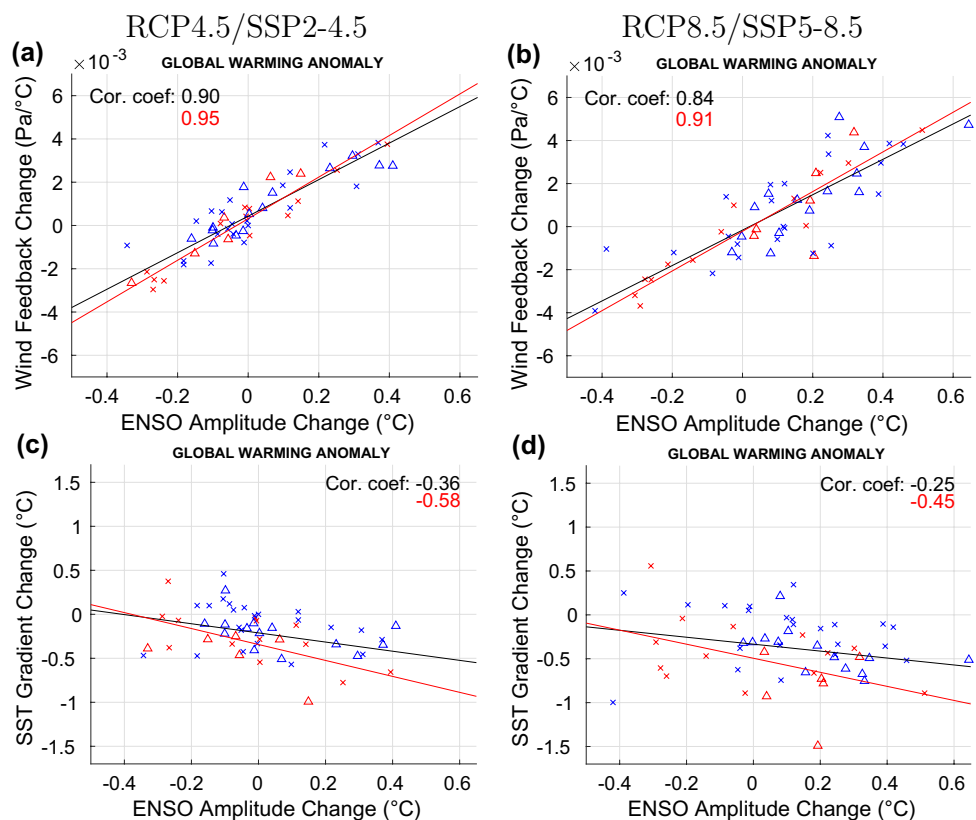
5 ENSO amplitude inter-model uncertainty source

Several studies have shown that ENSO amplitude is strongly influenced by the background mean state (Knutson et al. 1997; McPhaden et al. 2011; Hu et al. 2013; Kim et al. 2014a) and the wind-SST feedback (Lloyd et al. 2009; Vijayeta and Dommenges 2018). The background mean state has an influence on ENSO amplitude via the strength of the surface–subsurface coupling (Hu et al. 2013). Changes on climatological trade winds, which affect zonal SST gradient, vary the response of the zonal thermocline slope to zonal wind anomalies (Kim et al. 2014a). In the framework of the recharge oscillator model, Vijayeta and Dommenges (2018) could show under present day condition that the wind-SST feedback has the strongest influence on ENSO amplitude. Although ENSO is a complex phenomenon, we only focus in the following on these two factors to get insight into origin of the inter-model spread.

In Fig. 11a, b), we show the global warming signal of the ENSO amplitude and the wind-SST feedback. A strong positive linear relationship is detected with correlation coefficients of 0.90 (RCP4.5/SSP2-4.5, Fig. 11a) and 0.84 (RCP8.5/SSP5-8.5, Fig. 11b). In “Strong” (red color), the correlation coefficients amount to 0.95 and 0.91, respectively.

The relationship between the projected ENSO amplitude change and the zonal SST gradient is not as strong. While model ensemble exhibits a large spread of ENSO amplitude change, most of them project a decrease of the zonal SST gradient (Fig. 11c, d). The correlation coefficients are for -0.36 (RCP4.5/SSP2-4.5) and -0.25 (RCP8.5/SSP5-8.5). The “Strong” sub-ensemble models show an improved correlation of -0.58 and -0.45 . When calculating the SST gradient with different box averages, the results are virtually unchanged. Therefore, we conclude that the change in

Fig. 11 Inter-model relationship between the global warming signal of the ENSO amplitude change (x-axis) and; **a, b** the zonal wind stress-SST feedback change; **c, d** the Pacific equatorial mean zonal SST gradient change (y-axis) for; **a, c** RCP4.5/SSP2-4.5 scenario, and **b, d** RCP8.5/SSP5-8.5 scenario; crosses indicate CMIP5 models and triangles CMIP6 models; red corresponds to “Strong” sub-ensemble; the correlation with a 95% confidence level is shown



wind-SST feedback is an important factor of ENSO amplitude under global warming.

6 Summary and discussion

Using a CMIP5 and CMIP6 multi-model ensemble, the global warming signal in projected ENSO amplitude and the corresponding uncertainties have been quantified. The uncertainties have been split into the model uncertainty (spread of ENSO amplitude change within the ensemble), scenario uncertainty (spread of ENSO amplitude change caused by the different scenarios), and internal variability uncertainty (spread due to decadal ENSO variability). CMIP5 and CMIP6 models highly disagree with respect to future ENSO amplitude change. Projected changes range from decreasing to increasing ENSO amplitude (from -0.4 to $+0.6$ °C), with the mean global warming signal averaged over all models and scenarios close to zero.

Many state-of-the-art coupled climate models fail to simulate realistic ENSO characteristics. Therefore, models with realistic ENSO feedbacks and thus possibly realistic ENSO dynamics have been identified and grouped into the “Strong” sub-ensemble. The “Strong” sub-ensemble contains the models that are able to simulate the non-linearity

of ENSO most realistically (Cai et al. 2020; Hayashi et al. 2020). We also have investigated the unforced decadal variability of the ENSO amplitude. From this latter analysis, three additional sub-ensembles have been formed: models with high and low interannual and decadal ENSO variability, termed “High” and “Low”, respectively, and models with moderate interannual and decadal ENSO variability, termed “Moderate”. The later sub-ensemble is the closest to the observed ENSO variability.

Within CMIP5 models, the “High” sub-ensemble projects a reduction of the ENSO amplitude towards the end of the twenty-first century, while “Moderate” and “Low” sub-ensembles indicate an increase. When only considering realistic ENSO dynamic models, the “Strong” sub-ensemble, the signal is intensified: the negative and positive changes of the ENSO amplitude are increased both for “High” and “Moderate”, respectively. The result is consistent between scenarios: the signal is stronger for the RCP8.5 scenario than for the RCP4.5. In contrast, most of CMIP6 models under SSP5-8.5 scenario project an increase in ENSO amplitude towards the end of the twenty-first century, in agreement with recent studies (Fredriksen et al. 2020). The strongest increase is projected by models with high interannual and decadal ENSO variability. When considering the “Strong” sub-ensemble, the positive signal of ENSO amplitude

change is reduced. In this case, the result is not consistent between the scenarios: models under SSP2-4.5 scenario project a decrease of the ENSO amplitude. At this point, we must keep in mind that in this study we have been able to use 20 CMIP6 models in comparison to 36 CMIP5 models. Looking into models with weak ENSO atmospheric feedbacks, all sub-ensembles besides “Moderate” in CMIP5 show a stronger positive ENSO amplitude change than “Strong” models. In conclusion, the global warming signal of ENSO amplitude highly varies between CMIP5 and CMIP6, and the studied sub-ensembles.

The total uncertainty in the projected ENSO amplitude change obtained from all CMIP5 and CMIP6 models exhibits an increase over time: 0.11 °C at the beginning to 0.35 °C towards the end of the twenty-first century. Internal variability is the main contributor to the total uncertainty during the first three decades. The inter-model differences dominate thereafter, while scenario uncertainty is relatively small throughout the entire twenty-first century. CMIP6 models show a larger uncertainty than CMIP5 models. Although the model uncertainty is decreased, the scenario uncertainty is considerably increased (from 0.04 to 0.12 °C). This is in general agreement with previous studies indicating a greater climate sensitivity for CMIP6 models (Meehl et al. 2020). The largest uncertainty within a sub-ensemble is observed in “High”, approximating to 0.4 °C, and the smallest uncertainty when combining “Strong” and “Moderate” (about 0.3 °C). However, as shown by the signal-to-noise ratio, the global warming signal in the projected ENSO amplitude change is too small to be robustly detectable.

Finally, we have investigated two potential sources for the strong inter-model differences. The model spread is highly correlated with the spread in wind-SST feedback change, with a correlation coefficient of 0.90 and 0.84 for RCP4.5/SSP2-4.5 and RCP8.5/SSP5-8.5 scenarios, respectively. This suggests that it is important to understand the factors determining the wind-SST feedback under global warming to reduce uncertainty in ENSO-amplitude projections. However, from our analysis one cannot assure that the wind feedback is the dominant contributor to the future ENSO amplitude change, as it might partially be canceled by the change of the thermodynamic negative feedback, e.g., the shortwave feedback. A quantitative comparison between the positive and the negative feedback in terms of the ENSO amplitude change is out of scope of this paper. The correlation with the change in mean zonal SST gradient is of -0.36 and -0.25 . While most of the models agree on the reduction of the mean zonal SST gradient under global warming, the response of the wind feedback is extremely model dependent. This discrepancy between the mean state changes and the wind feedback changes is a puzzling question that needs to be answered in the future. A previous study has shown that there is a non-linear relation between mean-state

changes and ENSO amplitude, in which ENSO amplitude increases till an optimum and then decreases again (Hu et al. 2013). Considering the large mean state biases present in climate models, this might explain why the ENSO amplitude change varies to a similar mean state changes. In fact, if we consider realistic ENSO dynamic models, which show the smallest Niño4 SST bias, the inter-model correlation with SST gradient change is increased to -0.58 . In addition, the wind-SST feedback strength is strongly linked to the rising branch of the Walker Circulation, which again highly depends on the mean state (Bayr et al. 2020). Similarly, there is an ongoing debate about how the Walker Circulation will change under global warming (Knutson et al. 1997; Vecchi and Soden 2007; DiNezio et al. 2009, 2013; Sohn and Park 2010; Yu and Zwiers 2010; Power and Kociuba 2010, 2011; Meng et al. 2012; Luo et al. 2012; L’Heureux et al. 2013; Bayr et al. 2014). Thus, it is of great importance to improve the present mean state model biases, to understand how the Walker Circulation will change under global warming, and how this will affect ENSO amplitude.

Acknowledgements We acknowledge the World Climate Research Program’s Working Group on Coupled Modeling, the individual modeling groups of the Coupled Model Intercomparison Project (CMIP5, CMIP6), the UKMetOffice, ECMWF and NOAA for providing the data sets. This work was supported by the SFB 754 “Climate-Biochemistry Interactions in the tropical Ocean”, the Deutsche Forschungs Gemeinschaft (DFG) project “Influence of Model Bias on ENSO Projections of the 21st Century” through grant 429334714, and the BMBF project InterDec (Grant 01LP1609B).

Funding Open Access funding enabled and organized by Projekt DEAL.

Open Access This article is licensed under a Creative Commons Attribution 4.0 International License, which permits use, sharing, adaptation, distribution and reproduction in any medium or format, as long as you give appropriate credit to the original author(s) and the source, provide a link to the Creative Commons licence, and indicate if changes were made. The images or other third party material in this article are included in the article’s Creative Commons licence, unless indicated otherwise in a credit line to the material. If material is not included in the article’s Creative Commons licence and your intended use is not permitted by statutory regulation or exceeds the permitted use, you will need to obtain permission directly from the copyright holder. To view a copy of this licence, visit <http://creativecommons.org/licenses/by/4.0/>.

References

- Andrews T, Gregory JM, Webb MJ, Taylor KE (2012) Forcing, feedbacks and climate sensitivity in CMIP5 coupled atmosphere-ocean climate models. *Geophys Res Lett* 39:1–7. <https://doi.org/10.1029/2012GL051607>
- Bayr T, Dommenges D, Martin T, Power SB (2014) The eastward shift of the Walker Circulation in response to global warming and its relationship to ENSO variability. *Clim Dyn* 43:2747–2763. <https://doi.org/10.1007/s00382-014-2091-y>

- Bayr T, Latif M, Dommenget D et al (2018) Mean-state dependence of ENSO atmospheric feedbacks in climate models. *Clim Dyn* 50:3171–3194. <https://doi.org/10.1007/s00382-017-3799-2>
- Bayr T, Wengel C, Latif M et al (2019) Error compensation of ENSO atmospheric feedbacks in climate models and its influence on simulated ENSO dynamics. *Clim Dyn* 53:155–172. <https://doi.org/10.1007/s00382-018-4575-7>
- Bayr T, Dommenget D, Latif M (2020) Walker circulation controls ENSO atmospheric feedbacks in uncoupled and coupled climate model simulations. *Clim Dyn*. <https://doi.org/10.1007/s00382-020-05152-2>
- Bellenger H, Guilyardi E, Leloup J et al (2014) ENSO representation in climate models: from CMIP3 to CMIP5. *Clim Dyn* 42:1999–2018. <https://doi.org/10.1007/s00382-013-1783-z>
- Bjerknes J (1969) Atmospheric teleconnections from the equatorial Pacific. *Mon Weather Rev* 97:163–172. [https://doi.org/10.1175/1520-0493\(1969\)097%3c0163:atfep%3e2.3.co;2](https://doi.org/10.1175/1520-0493(1969)097%3c0163:atfep%3e2.3.co;2)
- Brown J, Brierley C, An S-I et al (2020) Comparison of past and future simulations of ENSO in CMIP5/PMIP3 and CMIP6/PMIP4 models. *Clim Past Discuss*. <https://doi.org/10.5194/cp-2019-155>
- Cai W, Wang G, Santos A et al (2015) Increased frequency of extreme La Niña events under greenhouse warming. *Nat Clim Chang* 5:132–137. <https://doi.org/10.1038/nclimate2492>
- Cai W, Ng B, Geng T et al (2020) Butterfly effect and a self-modulating El Niño response to global warming. *Nature* 585:68–73. <https://doi.org/10.1038/s41586-020-2641-x>
- Capotondi A, Wittenberg AT, Newman M et al (2015) Understanding ENSO diversity. *Bull Am Meteorol Soc* 96:921–938. <https://doi.org/10.1175/BAMS-D-13-00117.1>
- Cobb KM, Westphal N, Sayani HR et al (2013) Highly variable El Niño-Southern Oscillation throughout the Holocene. *Science* (80–) 339:67–70. <https://doi.org/10.1126/science.1228246>
- Cole J (2001) A slow dance for El Niño. *Science* (80–) 291:1496–1497
- Collins M, II AS, Cai W et al (2010) The impact of global warming on the tropical Pacific Ocean and El Niño. *Nat Geosci* 3:391–397. <https://doi.org/10.1038/ngeo868>
- Dee DP, Uppala SM, Simmons AJ et al (2011) The ERA-Interim reanalysis: Configuration and performance of the data assimilation system. *Q J R Meteorol Soc* 137:553–597. <https://doi.org/10.1002/qj.828>
- DiNezio PN, Clement AC, Vecchi GA et al (2009) Climate response of the equatorial Pacific to global warming. *J Clim* 22:4873–4892. <https://doi.org/10.1175/2009JCLI2982.1>
- DiNezio PN, Vecchi GA, Clement AC (2013) Detectability of changes in the walker circulation in response to global warming. *J Clim* 26:4038–4048. <https://doi.org/10.1175/JCLI-D-12-00531.1>
- Dommenget D (2010) The slab ocean El Niño. *Geophys Res Lett*. <https://doi.org/10.1029/2010GL044888>
- Dommenget D, Haase S, Bayr T, Frauen C (2014) Analysis of the Slab Ocean El Niño atmospheric feedbacks in observed and simulated ENSO dynamics. *Clim Dyn* 42:3187–3205. <https://doi.org/10.1007/s00382-014-2057-0>
- Eyring V, Bony S, Meehl GA et al (2016) Overview of the Coupled Model Intercomparison Project Phase 6 (CMIP6) experimental design and organization. *Geosci Model Dev* 9:1937–1958. <https://doi.org/10.5194/gmd-9-1937-2016>
- Fedorov AV, Philander SG (2000) Is El Niño changing? *Science* (80–) 288:1997–2002
- Fredriksen HB, Berner J, Subramanian AC, Capotondi A (2020) How does El Niño-Southern Oscillation change under global warming—a first look at CMIP6. *Geophys Res Lett*. <https://doi.org/10.1029/2020GL090640>
- Gidden MJ, Riahi K, Smith SJ et al (2019) Global emissions pathways under different socioeconomic scenarios for use in CMIP6: a dataset of harmonized emissions trajectories through the end of the century. *Geosci Model Dev* 12:1443–1475. <https://doi.org/10.5194/gmd-12-1443-2019>
- Guan C, McPhaden MJ (2016) Ocean processes affecting the twenty-first-century shift in ENSO SST variability. *J Clim* 29:6861–6879. <https://doi.org/10.1175/JCLI-D-15-0870.1>
- Guilyardi E, Wittenberg A, Fedorov A et al (2009) Understanding El Niño in ocean-atmosphere general circulation models: progress and challenges. *Bull Am Meteorol Soc* 90:325–340
- Hawkins E, Sutton R (2009) The potential to narrow uncertainty in regional climate predictions. *Bull Am Meteorol Soc* 90:1095–1107. <https://doi.org/10.1175/2009BAMS2607.1>
- Hayashi M, Jin FF, Stuecker MF (2020) Dynamics for El Niño-La Niña asymmetry constrain equatorial-Pacific warming pattern. *Nat Commun* 11:1–10. <https://doi.org/10.1038/s41467-020-17983-y>
- Hu ZZ, Kumar A, Ren HL et al (2013) Weakened interannual variability in the tropical Pacific ocean since 2000. *J Clim* 26:2601–2613. <https://doi.org/10.1175/JCLI-D-12-00265.1>
- Hu ZZ, Kumar A, Huang B et al (2017) Interdecadal variations of ENSO around 1999/2000. *J Meteorol Res* 31:73–81. <https://doi.org/10.1007/s13351-017-6074-x>
- Jin FF (1997) An equatorial ocean recharge paradigm for ENSO. Part I: conceptual model. *J Atmos Sci* 54:811–829. [https://doi.org/10.1175/1520-0469\(1997\)054%3c0811:AEORP%3e2.0.CO;2](https://doi.org/10.1175/1520-0469(1997)054%3c0811:AEORP%3e2.0.CO;2)
- Jin FF, Kim ST, Bejarano L (2006) A coupled-stability index for ENSO. *Geophys Res Lett*. <https://doi.org/10.1029/2006GL027221>
- Khon VC, Schneider B, Latif M et al (2018) Evolution of eastern equatorial Pacific seasonal and interannual variability in response to orbital forcing during the Holocene and Eemian from model simulations. *Geophys Res Lett* 45:9843–9851. <https://doi.org/10.1029/2018GL079337>
- Kim ST, Cai W, Jin FF et al (2014a) Response of El Niño sea surface temperature variability to greenhouse warming. *Nat Clim Chang* 4:786–790. <https://doi.org/10.1038/nclimate2326>
- Kim ST, Cai W, Jin FF, Yu JY (2014b) ENSO stability in coupled climate models and its association with mean state. *Clim Dyn* 42:3313–3321. <https://doi.org/10.1007/s00382-013-1833-6>
- Knutson TR, Manabe S, Gu D (1997) Simulated ENSO in a global coupled ocean-atmosphere model: multidecadal amplitude modulation and CO₂ sensitivity. *J Clim* 10:138–161. [https://doi.org/10.1175/1520-0442\(1997\)010%3c0138:SEIAGC%3e2.0.CO;2](https://doi.org/10.1175/1520-0442(1997)010%3c0138:SEIAGC%3e2.0.CO;2)
- Knutti R, Sedláček J (2013) Robustness and uncertainties in the new CMIP5 climate model projections. *Nat Clim Chang* 3:369–373. <https://doi.org/10.1038/nclimate1716>
- Koutavas A, DeMenocal PB, Olive GC, Lynch-Stieglitz J (2006) Mid-Holocene El Niño-Southern Oscillation (ENSO) attenuation revealed by individual foraminifera in eastern tropical Pacific sediments. *Geology* 34:993–996. <https://doi.org/10.1130/G22810A.1>
- L'Heureux ML, Lee S, Lyon B (2013) Recent multidecadal strengthening of the Walker circulation across the tropical Pacific. *Nat Clim Chang* 3:571–576. <https://doi.org/10.1038/nclimate1840>
- Latif M, Semenov VA, Park W (2015) Super El Niños in response to global warming in a climate model. *Clim Change* 132:489–500. <https://doi.org/10.1007/s10584-015-1439-6>
- Li J, Xie SP, Cook ER et al (2013) El Niño modulations over the past seven centuries. *Nat Clim Chang* 3:822–826. <https://doi.org/10.1038/nclimate1936>
- Lloyd J, Guilyardi E, Weller H, Slingo J (2009) The role of atmosphere feedbacks during ENSO in the CMIP3 models. *Atmos Sci Lett* 10:170–176. <https://doi.org/10.1002/asl.227>
- Lloyd J, Guilyardi E, Weller H (2011) The role of atmosphere feedbacks during ENSO in the CMIP3 models. Part II: using AMIP runs to understand the heat flux feedback mechanisms. *Clim Dyn* 37:1271–1292. <https://doi.org/10.1007/s00382-010-0895-y>
- Lloyd J, Guilyardi E, Weller H (2012) The role of atmosphere feedbacks during ENSO in the CMIP3 models. Part III: the shortwave

- flux feedback. *J Clim* 25:4275–4293. <https://doi.org/10.1175/JCLI-D-11-00178.1>
- Lübbecke JF, McPhaden MJ (2013) A comparative stability analysis of Atlantic and Pacific Niño modes. *J Clim* 26:5965–5980. <https://doi.org/10.1175/JCLI-D-12-00758.1>
- Luo JJ, Sasaki W, Masumoto Y (2012) Indian Ocean warming modulates Pacific climate change. *Proc Natl Acad Sci USA* 109:18701–18706. <https://doi.org/10.1073/pnas.1210239109>
- Maher N, Matei D, Milinski S, Marotzke J (2018) ENSO change in climate projections: forced response or internal variability? *Geophys Res Lett* 45:11–390
- McGregor HV, Fischer MJ, Gagan MK et al (2013) A weak El Niño/Southern Oscillation with delayed seasonal growth around 4,300 years ago. *Nat Geosci* 6:949–953. <https://doi.org/10.1038/ngeo1936>
- McPhaden MJ, Zebiak SE, Glantz MH (2006) ENSO as an integrating concept in earth science. *Science* (80–) 314:1740–1745
- McPhaden MJ, Lee T, McClurg D (2011) El Niño and its relationship to changing background conditions in the tropical Pacific Ocean. *Geophys Res Lett*. <https://doi.org/10.1029/2011GL048275>
- Meehl GA, Covey C, Delworth T et al (2007) The WCRP CMIP3 multimodel dataset: a new era in climate change research. *Bull Am Meteorol Soc* 88:1383–1394
- Meehl GA, Senior CA, Eyring V et al (2020) Context for interpreting equilibrium climate sensitivity and transient climate response from the CMIP6 Earth system models. *Sci Adv* 6:1–11. <https://doi.org/10.1126/sciadv.aba1981>
- Meinen CS, McPhaden MJ (2000) Observations of warm water volume changes in the equatorial Pacific and their relationship to El Niño and La Niña. *J Clim* 13:3551–3559. [https://doi.org/10.1175/1520-0442\(2000\)013%3c3551:OOWWVC%3e2.0.CO;2](https://doi.org/10.1175/1520-0442(2000)013%3c3551:OOWWVC%3e2.0.CO;2)
- Meng Q, Latif M, Park W et al (2012) Twentieth century Walker Circulation change: data analysis and model experiments. *Clim Dyn* 38:1757–1773. <https://doi.org/10.1007/s00382-011-1047-8>
- Philander SG (1989) El Niño, La Niña, and the Southern Oscillation. *Int Geophys Ser* 46:293. <https://doi.org/10.1126/scienc.248.4957.904>
- Planton YY, Guilyardi E, Wittenberg AT et al (2020) Evaluating climate models with the CLIVAR 2020 ENSO metrics package. *Bull Am Meteorol Soc*. <https://doi.org/10.1175/bams-d-19-0337.1>
- Power SB, Kociuba G (2010) The impact of global warming on the Southern Oscillation Index. *Clim Dyn* 37:1745–1754. <https://doi.org/10.1007/s00382-010-0951-7>
- Power SB, Kociuba G (2011) What caused the observed twentieth-century weakening of the walker circulation? *J Clim* 24:6501–6514. <https://doi.org/10.1175/2011JCLI4101.1>
- Rayner NA, Parker DE, Horton EB et al (2003) Global analyses of sea surface temperature, sea ice, and night marine air temperature since the late nineteenth century. *J Geophys Res Atmos*. <https://doi.org/10.1029/2002jd002670>
- Reintges A, Martin T, Latif M, Keenlyside NS (2017) Uncertainty in twenty-first century projections of the Atlantic Meridional Overturning Circulation in CMIP3 and CMIP5 models. *Clim Dyn* 49:1495–1511. <https://doi.org/10.1007/s00382-016-3180-x>
- Seager R, Cane M, Henderson N et al (2019) Strengthening tropical Pacific zonal sea surface temperature gradient consistent with rising greenhouse gases. *Nat Clim Chang* 9:517–522. <https://doi.org/10.1038/s41558-019-0505-x>
- Smith TM, Reynolds RW (2003) Extended reconstruction of global sea surface temperatures based on COADS data (1854–1997). *J Clim* 16:1495–1510. <https://doi.org/10.1175/1520-0442-16.10.1495>
- Sohn BJ, Park SC (2010) Strengthened tropical circulations in past three decades inferred from water vapor transport. *J Geophys Res Atmos*. <https://doi.org/10.1029/2009JD013713>
- Solomon S, Qin D, Manning M, Marquis M (2007) Climate change 2007: the physical science basis. Working group I contribution to the fourth assessment report of the IPCC. Intergov Panel Clim Chang (IPCC), Cambridge University Press, Cambridge 4
- Stevenson SL (2012) Significant changes to ENSO strength and impacts in the twenty-first century: results from CMIP5. *Geophys Res Lett*. <https://doi.org/10.1029/2012GL052759>
- Stocker TF, Qin D, Plattner G-K, et al (2013) Climate change 2013: The physical science basis. Contribution of working group I to the fifth assessment report of the intergovernmental panel on climate change. Intergov Panel Clim Chang (IPCC), Cambridge University Press, Cambridge, 1535
- Sun F, Yu JY (2009) A 10–15-Yr modulation cycle of ENSO intensity. *J Clim* 22:1718–1735. <https://doi.org/10.1175/2008JCLI2285.1>
- Taylor KE, Stouffer RJ, Meehl GA (2012) An overview of CMIP5 and the experiment design. *Bull Am Meteorol Soc* 93:485–498. <https://doi.org/10.1175/BAMS-D-11-00094.1>
- Timmermann A, Il AS, Kug JS et al (2018) El Niño–Southern Oscillation complexity. *Nature* 559:535–545
- Trenberth KE, Branstator GW, Karoly D et al (1998) Progress during TOGA in understanding and modeling global teleconnections associated with tropical sea surface temperatures. *J Geophys Res Ocean* 103:14291–14324. <https://doi.org/10.1029/97JC01444>
- Tudhope AW, Chilcott CP, McCulloch MT et al (2001) Variability in the El Niño–Southern Oscillation through a glacial–interglacial cycle. *Science* (80–) 291:1511–1517. <https://doi.org/10.1126/science.1057969>
- Uppala SM, Kållberg PW, Simmons AJ et al (2005) The ERA-40 re-analysis. *Q J R Meteorol Soc* 131:2961–3012. <https://doi.org/10.1256/qj.04.176>
- Vecchi GA, Soden BJ (2007) Global warming and the weakening of the tropical circulation. *J Clim* 20:4316–4340. <https://doi.org/10.1175/JCLI4258.1>
- Vijayeta A, Dommengat D (2018) An evaluation of ENSO dynamics in CMIP simulations in the framework of the recharge oscillator model. *Clim Dyn* 51:1753–1771. <https://doi.org/10.1007/s00382-017-3981-6>
- Wang Y, Luo Y, Lu J, Liu F (2019) Changes in ENSO amplitude under climate warming and cooling. *Clim Dyn* 52:1871–1882. <https://doi.org/10.1007/s00382-018-4224-1>
- Wengel C, Dommengat D, Latif M et al (2018) What controls ENSO-amplitude diversity in climate models? *Geophys Res Lett* 45:1989–1996. <https://doi.org/10.1002/2017GL076849>
- Wittenberg AT (2009) Are historical records sufficient to constrain ENSO simulations? *Geophys Res Lett* 36:1–5. <https://doi.org/10.1029/2009GL038710>
- Xu K, Huang QL, Tam CY et al (2019) Roles of tropical SST patterns during two types of ENSO in modulating wintertime rainfall over southern China. *Clim Dyn* 52:523–538. <https://doi.org/10.1007/s00382-018-4170-y>
- Yeh SW, Kirtman BP (2005) Pacific decadal variability and decadal ENSO amplitude modulation. *Geophys Res Lett* 32:1–5. <https://doi.org/10.1029/2004GL021731>
- Yu B, Zwiers FW (2010) Changes in equatorial atmospheric zonal circulations in recent decades. *Geophys Res Lett*. <https://doi.org/10.1029/2009GL042071>
- Zheng XT, Xie SP, Lv LH, Zhou ZQ (2016) Intermodel uncertainty in ENSO amplitude change tied to Pacific Ocean warming pattern. *J Clim* 29:7265–7279. <https://doi.org/10.1175/JCLI-D-16-0039.1>

Publisher's Note Springer Nature remains neutral with regard to jurisdictional claims in published maps and institutional affiliations.